

Saturated coordinated control of multiple underactuated unmanned surface vehicles over a closed curve

Lu LIU¹, Dan WANG^{1*}, Zhouhua PENG^{1,2*} & Hugh H.T. LIU³

¹*School of Marine Engineering, Dalian Maritime University, Dalian 116026, China;*

²*Department of Computer Science, City University of Hong Kong, Hong Kong, China;*

³*Institute for Aerospace Studies, University of Toronto, Toronto ON M3H 5T6, Canada*

Received November 30, 2016; accepted April 23, 2017; published online June 9, 2017

Abstract This paper presents a design method for saturated coordinated control of multiple underactuated unmanned surface vehicles (USVs) on a closed curve, holding a symmetric formation pattern. Each vehicle is subject to unknown sideslip, uncertain vehicle kinetics, and limited control torques. First, the course angle and surge velocity are considered as immediate signals to stabilize the along-track and cross-track path following errors. In the vehicle kinematics, a reduced-order extended state observer is utilized to compensate for the effect of the unknown sideslip. Next, a bounded neural network control law is constructed at the kinetic level with the aid of the a saturated function, a projection operator, and a dynamic surface design method. Finally, a parameter cyclic pursuit approach is presented to guarantee that the vehicles are evenly spaced over the closed curve for achieving a symmetric formation pattern. The input-to-state stability of the closed-loop system is analyzed via cascade theory. Comparative studies are given to show the effectiveness of the proposed method.

Keywords symmetric formation pattern, parameter cyclic pursuit, reduced-order extended state observer, neural networks, saturated control

Citation Liu L, Wang D, Peng Z H, et al. Saturated coordinated control of multiple underactuated unmanned surface vehicles over a closed curve. *Sci China Inf Sci*, 2017, 60(7): 070203, doi: 10.1007/s11432-016-9091-8

1 Introduction

Unmanned surface vehicles (USVs) have been playing an increasingly important role in military and civilian applications due to their small size, low cost, and high agility [1]. Studies on motion control of USVs have attracted great attention from various research communities. Current research goes beyond single USV control, and much attention has been paid to coordinated control of multiple USVs [2–25]. In general, coordinated USV systems can execute more challenging missions with improved mission performance, enhanced reliability against system failures, and reduced operational costs [1, 9, 17]. To achieve the coordination of multiple USVs, several methods have been proposed, including leader-follower formation control [2–8], cooperative trajectory tracking [9–15], and cooperative path following [16–25].

* Corresponding author (email: dwangdl@gmail.com, zhpeng@dlnu.edu.cn)

In particular, the objective of coordinated path following is to steer a group of vehicles along predefined path while keeping a desired formation [26,27].

Coordinated path following of USVs has been studied by many researchers [16–25]. In [16], a coordinated path following controller is proposed based on a passivity-based synchronization method. In [17], a coordinated path following design is presented for multiple autonomous vehicles in the presence of parametric uncertainty and unknown constant ocean currents. In [18], coordinated path following under discrete-time periodic communications is investigated. In [19], a coordinated path following controller is developed based on an adaptive dynamic surface control method and neural networks. In [20], coordinated path following control is addressed both for both state and output feedback. In [21], coordinated path following of marine vehicles with input saturation is investigated. In [22], a modular design approach is employed to develop distributed path following controllers where the path information is available for a small fraction of vehicles. In [23], a neurodynamics-based observer is developed to achieve the distributed output feedback path following control. In [16–23], a parallel formation pattern on multiple paths is achieved by synchronizing path variables. In [24,25], a path variable containment method is proposed to coordinate path following along one parameterized path, where the vehicles are evenly spaced between two virtual leaders along the path. All these coordinated path following controllers [16–25] focus on formation control over open curves. In many circumstances, closed paths are preferable by oceanographers, since the sensor measurements collected along repeated orbits can be interpreted without using a complex ocean model [28,29]. However, the existing methods on coordinated control of multiple USVs [16–25] cannot be applied to the coordinated control on a closed curve, since a symmetric formation pattern cannot be achieved by using the existing path variable synchronization method [16–23] and path variable containment method [24,25].

On the other hand, some efforts have been devoted to the coordinated control of moving sensor platforms [28–34]. In [28], a curve extension approach is presented for unit speed particles moving along a convex and closed loop. A formation motion is maintained by forcing the relative arc-length between each pair of vehicles to a constant value. It is later applied to underwater gliders and experimental results are given to verify its effectiveness [29]. In [30], a modified curve extension design method named concentric compression is proposed for unicycles on a set of convex and closed loops. The inter-vehicle formation is achieved by synchronizing the arc-lengths. In [31], the formation control problem for non-holonomic vehicles on convex orbits in a three-dimensional space is investigated with a time-varying reference orbital velocity. In [32], an adaptive formation controller is proposed for a group of fully actuated surface vessels to follow a set of convex orbit and maintain attitude synchronization. In [33], a formation of multi-unicycles around a closed curve is achieved in the presence of a time-invariant flow field. In [34], a formation controller is presented for underactuated ships along closed orbits. Note that most aforementioned studies focus on the parallel formations on multiple closed paths [30–34], which can be achieved by synchronizing the arc-lengths. Besides, the methods given in [28–34] require the communication to be bidirectional, which may be restrictive in practice.

Motivated by the above observations, we consider the coordinated control of multiple underactuated USVs over a closed curve. The USVs subject to unknown sideslip, dynamical uncertainties, and limited control torques. First, the course angle and surge velocity are treated as virtual controls to stabilize the along-track and cross-track path following errors. A reduced-order extended state observer is used to compensate for the effect of the unknown sideslip at the kinematics level. Second, a bounded neural network control law is developed at the kinetic level based on a dynamic surface control design method with the control torques known a priori. Third, a parameter cyclic pursuit approach is proposed to space the path variables such that a symmetric formation pattern is reached. The input-to-state stability of the closed-loop network is established via cascade theory. Comparison studies are given to illustrate the efficacy of the proposed method.

Compared with the existing results [16–25, 28–34], the main features of the proposed method are summarized as follows.

- A parameter cyclic pursuit approach is proposed to achieve a symmetric formation along a closed path. Different from the coordinated control of multiple USVs over multiple parameterized paths in [16–

23], a coordinated control along a parameterized path is considered here. Different from the coordinated control problem addressed in [24, 25], where the vehicles keep a queue formation along one open curve, a symmetric formation on a closed curve is achieved in this paper.

- In contrast to the coordinated controllers in [28–34], where the bidirectional communication is required, the communication graph is directed herein. Different from the parallel formations pattern on multiple closed curve considered in [30–34], a symmetric formation on a closed curve is achieved here.
- Compared with the coordinated controllers in [16–22, 24, 25, 28–34], where the input constraints are not considered, the developed coordinated controllers are bounded with the bounds known as a priori.

This paper is organized as follows. Section 2 introduces some preliminaries and gives the problem formulation. Section 3 presents the controller design and main results. Section 4 gives the simulation results to illustrate the proposed method. Section 5 concludes this paper.

2 Preliminaries and problem formulation

2.1 Preliminaries

Some graph concepts are briefly introduced. A graph $\mathcal{G} = \{\mathcal{V}, \mathcal{E}\}$ consists of a node set $\mathcal{V} = \{n_1, \dots, n_N\}$ and an edge set $\mathcal{E} = \{(n_i, n_j) \in \mathcal{E} \times \mathcal{E}\}$. The element (n_i, n_j) describes the communication from node i to node j . The adjacency matrix $\mathcal{A} = [a_{ij}] \in \mathbb{R}^{N \times N}$ associated with the graph \mathcal{G} is defined as $a_{ij} = 1$, if $(n_j, n_i) \in \mathcal{E}$; and $a_{ij} = 0$, otherwise. The Laplacian matrix \mathcal{L} associated with the graph \mathcal{G} is defined as $\mathcal{L} = \mathcal{D} - \mathcal{A}$ where $\mathcal{D} = \text{diag}\{d_1, \dots, d_N\}$ with $d_i = \sum_{j=1}^N a_{ij}$, $i = 1, \dots, N$.

Lemma 1 ([35]). Let \mathcal{G} be a weight-balanced and weakly connected graph, and \mathcal{L} be its Laplacian matrix. Then,

- The matrix $\text{Sym}(\mathcal{L}) := \frac{\mathcal{L} + \mathcal{L}^T}{2}$ is positive semi-definite.
- Denoted by λ^* the smallest nonzero eigenvalue of $\text{Sym}(\mathcal{L})$ and $\mathbf{1}_N = [1, \dots, 1]^T$, then $x^T \text{Sym}(\mathcal{L}) x \geq \lambda^* \|x - \frac{\mathbf{1}_N^T x}{N} \mathbf{1}_N\|^2$, for all $x \in \mathbb{R}^N$.

2.2 Problem formulation

Consider a group of N USVs, labeled as 1 to N . Let (x_i, y_i, ψ_{iB}) be the position and the yaw angle in a north-east frame, and let u_i, v_i, r_i be the surge, sway velocities and yaw rate in a body-fixed frame (see Figure 1). According to [36], the dynamical model of the i th USV can be described as

$$\begin{cases} \dot{x}_i = u_i \cos \psi_{iB} - v_i \sin \psi_{iB}, \\ \dot{y}_i = u_i \sin \psi_{iB} + v_i \cos \psi_{iB}, \\ \dot{\psi}_{iB} = r_i, \end{cases} \quad (1)$$

and

$$\begin{cases} m_{iu} \dot{u}_i = f_{iu}(u_i, v_i, r_i) + \tau_{iu} + \tau_{iuw}, \\ m_{iv} \dot{v}_i = f_{iv}(u_i, v_i, r_i) + \tau_{ivw}, \\ m_{ir} \dot{r}_i = f_{ir}(u_i, v_i, r_i) + \tau_{ir} + \tau_{irw}, \end{cases} \quad (2)$$

where m_{iu} , m_{iv} , and m_{ir} are inertial parameters; $f_{iu}(\cdot)$, $f_{iv}(\cdot)$, and $f_{ir}(\cdot)$ are unknown functions including Coriolis/centripetal force, and hydrodynamic damping effects; τ_{iuw} , τ_{ivw} , and τ_{irw} are ocean disturbances caused by wind, waves and currents; τ_{iu} and τ_{ir} are control inputs.

The kinematics (1) can be rewritten as

$$\begin{cases} \dot{x}_i = U_i \cos \psi_{iW}, \\ \dot{y}_i = U_i \sin \psi_{iW}, \\ \dot{\psi}_{iW} = r_i + \beta_{id}, \end{cases} \quad (3)$$

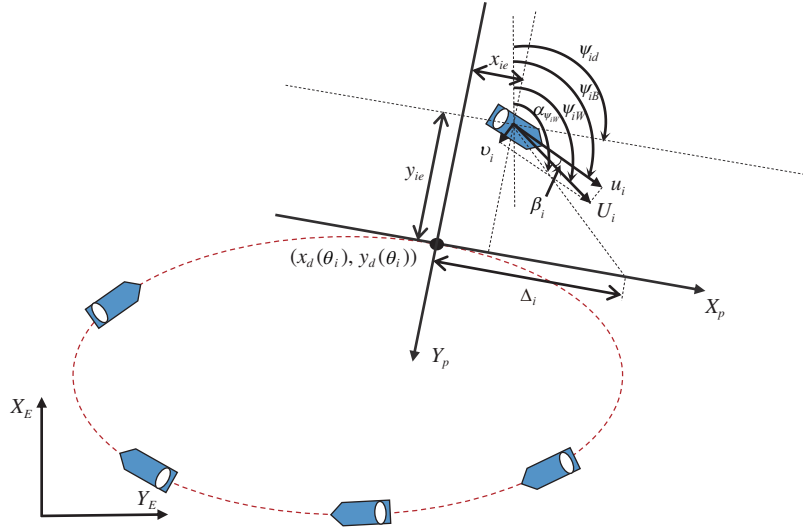


Figure 1 (Color online) A geometrical illustration of LOS guidance.

where $U_i = \sqrt{u_i^2 + v_i^2}$ is the total velocity of the vehicle, and is assumed to satisfy $U_i > 0$; $\psi_{iW} = \psi_{iB} + \beta_i$ is the course angle with $\beta_i = \text{atan2}(v_i/u_i)$ being an unknown sideslip angle, and $\beta_{id} = \dot{\beta}_i$.

Consider a closed curve that can be parameterized by

$$\begin{cases} x_d(\theta) = a \cos \theta + \mu b \sin \theta, \\ y_d(\theta) = b \sin \theta, \end{cases} \quad (4)$$

where θ is a time-independent variable; μ is the skew parameter; a is the semi-major axis length and b is the semi-minor axis length. Setting $a = b$ yields a circle and $a > b$ yields an ellipse.

For any given θ_i , the inertial position of the geometric path is denoted by $(x_d(\theta_i), y_d(\theta_i))$. The path-tangential angle is given by $\psi_{id} = \text{atan2}(y'_{id}, x'_{id})$, where $x'_{id} = \partial x_d(\theta_i)/\partial \theta_i$ and $y'_{id} = \partial y_d(\theta_i)/\partial \theta_i$. Then, for the i th USV located at (x_i, y_i) , the along-track error x_{ie} and cross-track error y_{ie} can be expressed in a path-tangential reference frame $\{P\}$ as follows:

$$\begin{bmatrix} x_{ie} \\ y_{ie} \end{bmatrix} = \begin{bmatrix} \cos \psi_{id} & -\sin \psi_{id} \\ \sin \psi_{id} & \cos \psi_{id} \end{bmatrix}^T \begin{bmatrix} x_i - x_d(\theta_i) \\ y_i - y_d(\theta_i) \end{bmatrix}. \quad (5)$$

Taking the time derivative of x_{ie} , y_{ie} and using (3), it follows that

$$\begin{cases} \dot{x}_{ie} = U_i \cos(\psi_{iW} - \psi_{id}) + \dot{\psi}_{id} y_{ie} - u_{id}^* \dot{\theta}_i, \\ \dot{y}_{ie} = U_i \sin(\psi_{iW} - \psi_{id}) - \dot{\psi}_{id} x_{ie}, \end{cases} \quad (6)$$

where $u_{id}^* = \sqrt{x_{id}^{\prime 2} + y_{id}^{\prime 2}}$.

Using the fact that $u_i = U_i \cos(\beta_i)$, we have $\dot{u}_i = \dot{U}_i \cos(\beta_i) + U_i \sin(\beta_i) \beta_{id} = \dot{U}_i - 2\dot{U}_i \sin(\frac{\beta_i}{2}) + U_i \sin(\beta_i) \beta_{id}$. Finally, the dynamics of x_{ie} , y_{ie} , ψ_{iW} , U_i , r_i can be expressed as

$$\begin{cases} \dot{x}_{ie} = U_i \cos(\psi_{iW} - \psi_{id}) + \dot{\psi}_{id} y_{ie} - u_{id}^* \dot{\theta}_i, \\ \dot{y}_{ie} = U_i \sin(\psi_{iW} - \psi_{id}) - \dot{\psi}_{id} x_{ie}, \\ \dot{\psi}_{iW} = r_i + \beta_{id}, \\ m_{iu} \dot{U}_i = f_{iu}(u_i, v_i, r_i) + \tau_{iu} + \tau_{iuw} + 2m_{iu} \dot{U}_i \sin\left(\frac{\beta_i}{2}\right) - m_{iu} U_i \sin(\beta_i) \beta_{id}, \\ m_{ir} \dot{r}_i = f_{ir}(u_i, v_i, r_i) + \tau_{ir} + \tau_{irw}. \end{cases} \quad (7)$$

The control objective is to develop a coordinated path following controller for the N USVs with the dynamics (1) and (2), such that the USVs follow the parameterized and closed path $(x_d(\theta), y_d(\theta))$ while achieving a symmetric formation on the path.

3 Controller design

3.1 Controller design

3.1.1 Step 1

In this step, the course angle ψ_{iW} and the surge speed U_i are treated as virtual controls to stabilize x_{ie} and y_{ie} .

Define $\psi_{ie} = \psi_{iW} - \alpha_{\psi_i}$, $z_{iu} = U_i - U_{ir}$, $q_{iu} = U_{ir} - \alpha_{U_i}$, $\tilde{z}_{iu} = \hat{z}_{iu} - z_{iu}$, where α_{ψ_i} and α_{U_i} are the virtual controls of ψ_i and U_i , respectively; U_{ir} is the estimation value of α_{U_i} ; \hat{z}_{iu} is the estimation of the tracking error z_{iu} . Then, we can write the first two equations of (7) as

$$\begin{cases} \dot{x}_{ie} = \alpha_{U_i} + z_{iu} + q_{iu} - 2U_i \sin^2\left(\frac{\psi_{iW} - \psi_{id}}{2}\right) + \dot{\psi}_{id} y_{ie} - u_{id}^* \dot{\theta}_i, \\ \dot{y}_{ie} = U_i \sin(\alpha_{\psi_i} - \psi_{id}) + \varrho_i - \dot{\psi}_{id} x_{ie}, \end{cases} \quad (8)$$

where $\varrho_i = U_i \sin(\psi_{iW} - \psi_{id}) - U_i \sin(\alpha_{\psi_i} - \psi_{id})$.

The virtual guidance laws for the i th vehicle is proposed as follows:

$$\begin{cases} \alpha_{\psi_i} = \psi_{id} + \arctan\left(-\frac{y_{ie}}{\Delta_i}\right), \\ \alpha_{U_i} = -k_{i1} x_{ie} / \Pi_{ix} + u_{id}^* \dot{\theta}_i + 2U_i \sin^2\left(\frac{\psi_{iW} - \psi_{id}}{2}\right) - \hat{z}_{iu}, \end{cases} \quad (9)$$

where Δ_i is a look ahead distance; k_{i1} is a positive constant; $\Pi_{ix} = \sqrt{x_{ie}^2 + \Delta_i^2}$ with Δ_{ix} being a positive constant.

Substituting (9) into (8) and using the fact $\sin(\arctan(-\frac{y_{ie}}{\Delta_i})) = -\frac{y_{ie}}{\Pi_{iy}}$ with $\Pi_{iy} = \sqrt{y_{ie}^2 + \Delta_i^2}$, it follows that the dynamics of x_{ie} and y_{ie} become

$$\begin{cases} \dot{x}_{ie} = -k_{i1} x_{ie} / \Pi_{ix} - \tilde{z}_{iu} + q_{iu} + \dot{\psi}_{id} y_{ie}, \\ \dot{y}_{ie} = -U_i y_{ie} / \Pi_{iy} + \varrho_i - \dot{\psi}_{id} x_{ie}. \end{cases} \quad (10)$$

3.1.2 Step 2

In this step, the yaw velocity r_i is viewed as a control input to stabilize ψ_{ie} .

Before starting, a reduced-order extended state observer is proposed to identify the uncertain kinematics β_{id} ,

$$\begin{cases} \dot{p}_i = -\omega_i p_i - \omega_i^2 \psi_{iW} - \omega_i r_i, \\ \dot{\hat{\beta}}_{id} = \omega_i \psi_{iW} + p_i, \end{cases} \quad (11)$$

where p_i is the auxiliary state of the observer; ω_i is a design parameter.

To move on, the following assumption is made.

Assumption 1. There exists a positive constant β^* such that $|\dot{\hat{\beta}}_{id}| \leq \beta^*$.

Let $\tilde{\beta}_{id} = \hat{\beta}_{id} - \beta_{id}$, whose derivative with (7) and (11) can be expressed as

$$\dot{\tilde{\beta}}_{id} = -\omega_i \tilde{\beta}_{id} - \dot{\beta}_{id}. \quad (12)$$

Define $z_{ir} = r_i - r_{ir}$, $q_{ir} = r_{ir} - \alpha_{r_i}$, $\tilde{z}_{ir} = \hat{z}_{ir} - z_{ir}$, where α_{r_i} is a virtual control law; r_{ir} represents the estimation of α_{r_i} ; \hat{z}_{ir} is the estimation of the tracking error z_{ir} . From (7), the dynamic of ψ_{ie} can be expressed as

$$\dot{\psi}_{ie} = \alpha_{r_i} + z_{ir} + q_{ir} + \beta_{id} - \dot{\alpha}_{\psi_i}. \quad (13)$$

A virtual control law α_{r_i} is given by

$$\alpha_{r_i} = -k_{i2} \psi_{ie} / \Pi_{i\psi} - \hat{\beta}_{id} + \dot{\alpha}_{\psi_i} - \frac{y_{ie} \varrho_i}{\psi_{ie}} - \hat{z}_{ir}, \quad (14)$$

where k_{i2} is a positive constant; $\Pi_{i\psi} = \sqrt{\psi_{ie}^2 + \Delta_{i\psi}^2}$ with $\Delta_{i\psi}$ being a positive constant.

Note that $\psi_{ie} = (\psi_{iW} - \psi_{id}) - (\alpha_{\psi_i} - \psi_{id})$, then we have $\lim_{\psi_{ie} \rightarrow 0} \frac{\sin(\psi_{iW} - \psi_{id}) - \sin(\alpha_{\psi_i} - \psi_{id})}{\psi_{ie}} = \cos(\alpha_{\psi_i} - \psi_{id})$, and $\lim_{\psi_{ie} \rightarrow 0} \frac{Q_i}{\psi_{ie}} = U_i \cos(\alpha_{\psi_i} - \psi_{id})$.

Substituting (14) into (13), the dynamic of ψ_{ie} becomes

$$\dot{\psi}_{ie} = -k_{i2}\psi_{ie}/\Pi_{i\psi} - \frac{y_{ie}Q_i}{\psi_{ie}} - \tilde{z}_{ir} + q_{ir} - \tilde{\beta}_{id}. \tag{15}$$

Introduce two new states U_{ir} and r_{ir} as the desired values of U_i and r_i , respectively. Let α_{U_i} and α_{r_i} pass through two first-order filters with time constants γ_{iu} and γ_{ir} to obtain U_{ir} and r_{ir} as follows:

$$\dot{U}_{ir} = \frac{\alpha_{U_i} - U_{ir}}{\gamma_{iu}}, \quad \dot{r}_{ir} = \frac{\alpha_{r_i} - r_{ir}}{\gamma_{ir}}. \tag{16}$$

The time derivatives of q_{iu} and q_{ir} are given by

$$\dot{q}_{iu} = -\frac{q_{iu}}{\gamma_{iu}} - \dot{\alpha}_{iU}, \quad \dot{q}_{ir} = -\frac{q_{ir}}{\gamma_{ir}} - \dot{\alpha}_{ir}. \tag{17}$$

By integration of (17), it follows that

$$q_{iu}(t) = e^{-\frac{t}{\gamma_{iu}}} q_{iu}(0) - \int_0^t e^{-\frac{t-\tau}{\gamma_{iu}}} \dot{\alpha}_{iU}(\tau) d\tau, \quad q_{ir}(t) = e^{-\frac{t}{\gamma_{ir}}} q_{ir}(0) - \int_0^t e^{-\frac{t-\tau}{\gamma_{ir}}} \dot{\alpha}_{ir}(\tau) d\tau, \tag{18}$$

from which we can compute an upper bound for q_{iu} and q_{ir} as

$$|q_{iu}(t)| \leq e^{-\frac{t}{\gamma_{iu}}} |q_{iu}(0)| + \gamma_{iu} \alpha_{iU}^*, \quad |q_{ir}(t)| \leq e^{-\frac{t}{\gamma_{ir}}} |q_{ir}(0)| + \gamma_{ir} \alpha_{ir}^*, \tag{19}$$

where $|\dot{\alpha}_{iU}|_\infty \leq \alpha_{iU}^*$, $|\dot{\alpha}_{ir}|_\infty \leq \alpha_{ir}^*$ with α_{iU}^* and α_{ir}^* being positive constants. Since the energy to drive the USV is limited and the derivatives of the reference path are bounded, the boundedness of $\dot{\alpha}_{iU}$ and $\dot{\alpha}_{ir}$ are naturally satisfied for marine vehicles. Then, there exist positive constants q_{iu}^* and q_{ir}^* such that $|q_{iu}(t)| \leq q_{iu}^*$ and $|q_{ir}(t)| \leq q_{ir}^*$.

3.1.3 Step 3

In this step, we aim to develop the kinetic controllers τ_{iu} and τ_{ir} based on the first-order filters (16).

From (7), the time derivative of z_{iu} and z_{ir} is given by

$$m_{iu} \dot{z}_{iu} = \bar{f}_{iu}(\cdot) + \tau_{iu}, \quad m_{ir} \dot{z}_{ir} = \bar{f}_{ir}(\cdot) + \tau_{ir}, \tag{20}$$

where $\bar{f}_{iu}(\cdot) = f_{iu}(u_i, v_i, r_i) + \tau_{iuw} + 2m_{iu} \dot{U}_i \sin(\frac{\beta_i}{2}) - m_{iu} U_i \sin(\beta_i) \beta_{id} - m_{iu} \dot{U}_{ir}$ and $\bar{f}_{ir}(\cdot) = f_{ir}(u_i, v_i, r_i) + \tau_{irw} - m_{ir} \dot{r}_{ir}$.

Note that the unknown functions $\bar{f}_{iu}(\cdot)$ and $\bar{f}_{ir}(\cdot)$ include both the state-related nonlinear uncertainty and the external disturbances. Two neural networks are employed to approximate the unknown functions

$$\bar{f}_{iu} = W_{iu}^T \sigma_{iu}(\xi_{iu}) + \varepsilon_{iu}, \quad \bar{f}_{ir} = W_{ir}^T \sigma_{ir}(\xi_{ir}) + \varepsilon_{ir}, \tag{21}$$

where $W_{iu} \in \mathbb{R}^s$ and $W_{ir} \in \mathbb{R}^s$ are the unknown time-varying matrixes satisfying $\|W_{iu}\| \leq W_{iu}^*$ and $\|W_{ir}\| \leq W_{ir}^*$ with W_{iu}^* and W_{ir}^* being positive constants; $\xi_{iu} = [z_{iu}(t), z_{iu}(t - t_d), \tau_{iu}, 1]^T \in \mathbb{R}^4$ and $\xi_{ir} = [z_{ir}(t), z_{ir}(t - t_d), \tau_{ir}, 1]^T \in \mathbb{R}^4$ are the input matrixes; $\sigma_{iu}(\xi_{iu}) : \mathbb{R}^4 \rightarrow \mathbb{R}^s$ and $\sigma_{ir}(\xi_{ir}) : \mathbb{R}^4 \rightarrow \mathbb{R}^s$ are known continuous basis vectors satisfying $\|\sigma_{iu}\| \leq \sigma_u^*$ and $\|\sigma_{ir}\| \leq \sigma_r^*$ with σ_u^* and σ_r^* being positive constants; ε_{iu} and ε_{ir} are the approximation errors satisfying $|\varepsilon_{iu}| \leq \varepsilon_{iu}^*$ and $|\varepsilon_{ir}| \leq \varepsilon_{ir}^*$ with ε_{iu}^* and ε_{ir}^* being positive constants.

A kinetic controller is constructed as follows:

$$\tau_{iu} = -k_{i3} \hat{z}_{iu} / \Pi_u - \hat{W}_{iu}^T \sigma_{iu}(\xi_{iu}), \quad \tau_{ir} = -k_{i4} \hat{z}_{ir} / \Pi_r - \hat{W}_{ir}^T \sigma_{ir}(\xi_{ir}), \tag{22}$$

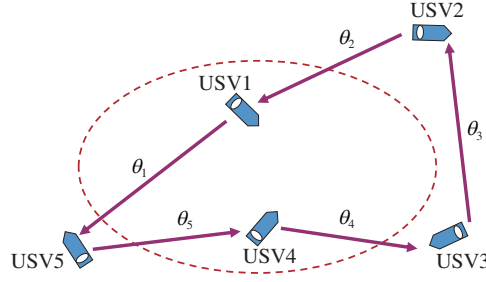


Figure 2 (Color online) Communication topology.

where k_{i3} and k_{i4} are control gains; $\Pi_{iu} = \sqrt{\hat{z}_{iu}^2 + \Delta_{iu}^2}$ and $\Pi_{ir} = \sqrt{\hat{z}_{ir}^2 + \Delta_{ir}^2}$ with Δ_{iu} and Δ_{ir} being positive constants; \hat{W}_{iu} and \hat{W}_{ir} are estimates of W_{iu} and W_{ir} , respectively. \hat{z}_{iu} and \hat{z}_{ir} are obtained from the following dynamical compensators as

$$\begin{cases} m_{iu}\dot{\hat{z}}_{iu} = -k_{i3}\hat{z}_{iu}/\Pi_u - (k_{i3} + \rho_{iu})(\hat{z}_{iu} - z_{iu}), \\ m_{ir}\dot{\hat{z}}_{ir} = -k_{i4}\hat{z}_{ir}/\Pi_r - (k_{i4} + \rho_{ir})(\hat{z}_{ir} - z_{ir}), \end{cases} \quad (23)$$

where ρ_{iu} and ρ_{ir} are positive constants.

The update laws for \hat{W}_{iu} and \hat{W}_{ir} are designed as

$$\dot{\hat{W}}_{iu} = -\Gamma_{iu}\text{Proj}(\hat{W}_{iu}, \sigma_{iu}(\xi_{iu})\tilde{z}_{iu}), \quad \dot{\hat{W}}_{ir} = -\Gamma_{ir}\text{Proj}(\hat{W}_{ir}, \sigma_{ir}(\xi_{ir})\tilde{z}_{ir}), \quad (24)$$

where Proj denotes the projection operator [37]; Γ_{iu} and Γ_{ir} are positive constants. Due to the projection operator, there exist positive constants ϱ_{i1} and ϱ_{i2} such that $\|\hat{W}_{iu}\| \leq W_{iu}^* + \varrho_{i1}$ and $\|\hat{W}_{ir}\| \leq W_{ir}^* + \varrho_{i2}$.

Let $\tilde{W}_{iu} = \hat{W}_{iu} - W_{iu}$ and $\tilde{W}_{ir} = \hat{W}_{ir} - W_{ir}$. Then, the dynamics of \tilde{z}_{iu} , \tilde{z}_{ir} , \tilde{W}_{iu} , and \tilde{W}_{ir} can be expressed as

$$\begin{cases} m_{iu}\dot{\tilde{z}}_{iu} = -(k_{i3} + \rho_{iu})\tilde{z}_{iu} + \tilde{W}_{iu}^T\sigma_{iu}(\xi_{iu}) - \varepsilon_{iu}, \\ m_{ir}\dot{\tilde{z}}_{ir} = -(k_{i4} + \rho_{ir})\tilde{z}_{ir} + \tilde{W}_{ir}^T\sigma_{ir}(\xi_{ir}) - \varepsilon_{ir}, \\ \dot{\tilde{W}}_{iu} = \Gamma_{iu}\sigma_{iu}(\xi_{iu})\tilde{z}_{iu}, \\ \dot{\tilde{W}}_{ir} = \Gamma_{ir}\sigma_{ir}(\xi_{ir})\tilde{z}_{ir}. \end{cases} \quad (25)$$

Note that a salient feature of the proposed control law (22) is that the control torques are bounded and the bounds are known a priori to a designer. The upper bound of the torque input is as follows:

$$|\tau_{iu}| \leq k_{i3} + \delta_{iu}\sigma_{iu}^*, \quad |\tau_{ir}| \leq k_{i4} + \delta_{ir}\sigma_{ir}^*, \quad (26)$$

where δ_{iu} and δ_{ir} are positive constants defined as $\delta_{iu} = W_{iu}^* + \varrho_{i1}$, $\delta_{ir} = W_{ir}^* + \varrho_{i2}$, which exist due to the use of projection operator.

3.1.4 Step 4

In this step, we aim to design an update law for θ_i such that a symmetric formation can be achieved.

The neighbor topology for the N USVs is defined according to their positions in circular clockwise radial order around the closed curve, and the i th USV only received the information from the one previous to it. For example, the communication topology among five vehicles is shown in Figure 2. Let the communication topology among USVs be described by a graph \mathcal{G} , and \mathcal{L} be its Laplacian matrix.

Let θ_i represent the path variable of the i th vehicle, and its updating law is to be designed. θ_{i+} denotes the path variable of the i th vehicle's neighboring vehicle, which is determined by the communication network. A coordination error based on neighbors' information is defined as

$$e_i = \theta_{i+} - \theta_i + \zeta_i, \quad (27)$$

where

$$\zeta_i = \begin{cases} 0, & \text{if } \theta_{i+} - \theta_i \geq 0, \\ 2\pi, & \text{if } \theta_{i+} - \theta_i < 0. \end{cases} \quad (28)$$

Then, an updating law for the path parameter θ_i is designed as

$$\dot{\theta}_i = -\kappa_i e_i, \quad (29)$$

where κ_i is a positive constant.

Letting $e = [e_1, \dots, e_N]^T$ and $\kappa = \text{diag}\{\kappa_i\}$, the error system in terms of x_{ie} , y_{ie} , ψ_{ie} , \hat{z}_{iu} , \hat{z}_{ir} and e can be expressed by

$$\begin{cases} \dot{x}_{ie} = -k_{i1}x_{ie}/\Pi_{ix} - \tilde{z}_{iu} + q_{iu} + \dot{\psi}_{id}y_{ie}, \\ \dot{y}_{ie} = -U_i y_{ie}/\Pi_{iy} + \varrho_i - \dot{\psi}_{id}x_{ie}, \\ \dot{\psi}_{ie} = -k_{i2}\psi_{ie}/\Pi_{i\psi} - \frac{y_{ie}\varrho_i}{\psi_{ie}} - \tilde{z}_{ir} + q_{ir} - \tilde{\beta}_{id}, \\ m_{iu}\dot{\hat{z}}_{iu} = -k_{i3}\hat{z}_{iu}/\Pi_{iu} - (k_{i3} + \rho_{iu})\tilde{z}_{iu}, \\ m_{ir}\dot{\hat{z}}_{ir} = -k_{i4}\hat{z}_{ir}/\Pi_{ir} - (k_{i4} + \rho_{ir})\tilde{z}_{ir}, \\ \dot{e} = -\mathcal{L}\kappa e. \end{cases} \quad (30)$$

3.2 Stability analysis

The closed-loop error system can be regarded as a cascade system formed by two estimation error subsystems (the subsystem (12) and subsystem (25)) and the tracking error subsystem (30). We first state the stability of the subsystem (12).

Lemma 2. The subsystem (12), viewed as a system with the states being $\tilde{\beta}_{id}$, the input being $\dot{\beta}_{id}$, is input-to-state stable (ISS).

Proof. Construct the following Lyapunov function:

$$V_{i1} = \frac{1}{2}\tilde{\beta}_{id}^2. \quad (31)$$

Taking the time derivative of V_{i1} along (12) results in

$$\dot{V}_{i1} = -\omega_i\tilde{\beta}_{id}^2 - \tilde{\beta}_{id}\dot{\beta}_{id}. \quad (32)$$

Since $|\tilde{\beta}_{id}| \geq \frac{|\dot{\beta}_{id}|}{\omega_i\theta_{i1}}$, we have

$$\dot{V}_{i1} \leq -\omega_i(1 - \theta_{i1})\tilde{\beta}_{id}^2, \quad (33)$$

where $0 < \theta_{i1} < 1$. Then we conclude that the system (12) is ISS, and

$$|\tilde{\beta}_{id}(t)| \leq \max \left\{ \varpi_{i1}(|\tilde{\beta}_{id}(0)|, t), \phi_i^{\beta_d}(|\dot{\beta}_{id}|) \right\}, \quad (34)$$

where ϖ_{i1} is a \mathcal{KL} function and $\phi_i^{\beta_d}(s) = (1/\omega_{i1}\theta_{i1})s$.

The following lemma presents the stability of the subsystem (25).

Lemma 3. The subsystem (25), viewed as a system with the states being \tilde{z}_{iu} , \tilde{z}_{ir} , \tilde{W}_{iu} and \tilde{W}_{ir} , the inputs being ε_{iu} , ε_{ir} , \tilde{W}_{iu} and \tilde{W}_{ir} , is ISS.

Proof. Construct the following Lyapunov function:

$$V_{i2} = \frac{1}{2}m_{iu}\tilde{z}_{iu}^2 + \frac{1}{2}m_{ir}\tilde{z}_{ir}^2 + \frac{1}{2}\tilde{W}_{iu}^T\Gamma_{iu}^{-1}\tilde{W}_{iu} + \frac{1}{2}\tilde{W}_{ir}^T\Gamma_{ir}^{-1}\tilde{W}_{ir}, \quad (35)$$

whose time derivative along (25) satisfies

$$\begin{aligned} \dot{V}_{i2} &= -E_{i1}^T K_{i1} E_{i1} + h_{i1}^T E_{i1} \\ &\leq -\lambda_{\min}(K_{i1}) \|E_{i1}\|^2 - \lambda_{\min}(K_{i1}) \|\tilde{W}_{iu}\|^2 - \lambda_{\min}(K_{i1}) \|\tilde{W}_{ir}\|^2 \\ &\quad + h_{i1}^T E_{i1} + \lambda_{\min}(K_{i1}) \|\tilde{W}_{iu}\|^2 + \lambda_{\min}(K_{i1}) \|\tilde{W}_{ir}\|^2 \\ &\leq -\lambda_{\min}(K_{i1}) \|E_{i2}\|^2 + \|h_{i2}\| \|E_{i2}\|, \end{aligned} \tag{36}$$

where $K_{i1} = \text{diag}\{k_{i3} + \varrho_{iu}, k_{i4} + \varrho_{ir}\}$, $E_{i1} = [\tilde{z}_{iu}, \tilde{z}_{ir}]^T$, $h_{i1} = [\varepsilon_{iu}, \varepsilon_{ir}]^T$, $E_{i2} = [\tilde{z}_{iu}, \tilde{z}_{ir}, \|\tilde{W}_{iu}\|, \|\tilde{W}_{ir}\|]^T$, $h_{i2} = [|\varepsilon_{iu}|, |\varepsilon_{ir}|, \lambda_{\min}(K_{i1}) \|\tilde{W}_{iu}\|, \lambda_{\min}(K_{i1}) \|\tilde{W}_{ir}\|]^T$.

Since $\|E_{i2}\| \geq \frac{|\varepsilon_{iu}|}{\theta_{i2} \lambda_{\min}(K_{i1})} + \frac{|\varepsilon_{ir}|}{\theta_{i2} \lambda_{\min}(K_{i1})} + \frac{\|\tilde{W}_{iu}\|}{\theta_{i2}} + \frac{\|\tilde{W}_{ir}\|}{\theta_{i2}} \geq \frac{\|h_{i2}\|}{\theta_{i2} \lambda_{\min}(K_{i1})}$, we have

$$\dot{V}_{i2} \leq -(1 - \theta_{i2}) \lambda_{\min}(K_{i1}) \|E_{i2}\|^2, \tag{37}$$

where $0 < \theta_{i2} < 1$. It follows that the subsystem (25) is ISS, and

$$\|E_{i2}(t)\| \leq \max \left\{ \varpi_{i2}(\|E_{i2}(0)\|, t), \phi_i^{\varepsilon_u}(|\varepsilon_u|) + \phi_i^{\varepsilon_r}(|\varepsilon_r|) + \phi_i^{W_u}(\|W_u\|) + \phi_i^{W_r}(\|W_r\|) \right\}, \tag{38}$$

where ϖ_{i2} is a \mathcal{KL} function and $\phi_i^{\varepsilon_u}(s) = \sqrt{\frac{\lambda_{\max}(S_{i1})}{\lambda_{\min}(S_{i1})}} \frac{s}{\theta_{i2} \lambda_{\min}(K_{i1})}$, $\phi_i^{\varepsilon_r}(s) = \sqrt{\frac{\lambda_{\max}(S_{i1})}{\lambda_{\min}(S_{i1})}} \frac{s}{\theta_{i2} \lambda_{\min}(K_{i1})}$, $\phi_i^{W_u}(s) = \sqrt{\frac{\lambda_{\max}(S_{i1})}{\lambda_{\min}(S_{i1})}} \frac{s}{\theta_{i2}}$, $\phi_i^{W_r}(s) = \sqrt{\frac{\lambda_{\max}(S_{i1})}{\lambda_{\min}(S_{i1})}} \frac{s}{\theta_{i2}}$ with $S_{i1} = \text{diag}\{m_{iu}, m_{ir}, \Gamma_{iu}^{-1}, \Gamma_{ir}^{-1}\}$. The boundedness of \tilde{W}_{iu} and \tilde{W}_{ir} is guaranteed by projection operation [38], and their upper bounds are given by $\|\tilde{W}_{iu}\| \leq 2W_{iu}^* + \varrho_{i1}$ and $\|\tilde{W}_{ir}\| \leq 2W_{ir}^* + \varrho_{i2}$.

Next, the stability of the tracking error subsystem (30) is stated as follows.

Lemma 4. The subsystem (30), viewed as a system with the states being $x_{ie}, y_{ie}, \psi_{ie}, \hat{z}_{iu}, \hat{z}_{ir}$ and e_i , the inputs being $\tilde{\beta}_{id}, \tilde{z}_{iu}, \tilde{z}_{ir}, q_{iu}$ and q_{ir} , is ISS.

Proof. Construct the following Lyapunov function:

$$V_3 = \sum_{i=1}^N \left\{ \frac{1}{2} x_{ie}^2 + \frac{1}{2} y_{ie}^2 + \frac{1}{2} \psi_{ie}^2 + \frac{1}{2} m_{iu} \hat{z}_{iu}^2 + \frac{1}{2} m_{ir} \hat{z}_{ir}^2 + \frac{1}{2} e_i^2 \right\}. \tag{39}$$

Substituting (30) into the derivative of V_3 , we have

$$\begin{aligned} \dot{V}_3 &= \sum_{i=1}^N \left\{ -k_{i1} x_{ie}^2 / \Pi_{ix} + x_{ie}(-\tilde{z}_{iu} + q_{iu}) - U_i y_{ie}^2 / \Pi_{iy} - k_{i2} \psi_{ie}^2 / \Pi_{i\psi} + \psi_{ie}(-\tilde{z}_{ir} + q_{ir} - \tilde{\beta}_{id}) \right. \\ &\quad \left. - k_{i3} \hat{z}_{iu}^2 / \Pi_{iu} - (k_{i3} + \rho_{iu}) \hat{z}_{iu} \tilde{z}_{iu} - k_{i4} \hat{z}_{ir}^2 / \Pi_{ir} - (k_{i4} + \rho_{ir}) \hat{z}_{ir} \tilde{z}_{ir} \right\} - e^T \mathcal{L} \kappa e \\ &\leq \sum_{i=1}^N \left\{ -\frac{\lambda_{\min}(K_{i2}) \|E_{i3}\|^2}{\sqrt{\|E_{i3}\|^2 + \Delta_{i \max}^2}} + \|h_{i3}\| \|E_{i3}\| \right\} - e^T \left(\frac{\mathcal{L} + \mathcal{L}^T}{2} \right) \kappa e, \end{aligned} \tag{40}$$

where $K_{i2} = \text{diag}\{k_{i1}, U_i, k_{i2}, k_{i3}, k_{i4}\}$, $E_{i3} = [x_{ie}, y_{ie}, \psi_{ie}, \hat{z}_{iu}, \hat{z}_{ir}]^T$, $\Delta_{i \max} = \max\{\Delta_{ix}, \Delta_{iy}, \Delta_{i\psi}, \Delta_{iu}, \Delta_{ir}\}$ and $h_{i3} = [|\tilde{z}_{iu}| + |q_{iu}|, |\tilde{z}_{ir}| + |q_{ir}| + |\tilde{\beta}_{id}|, (k_{i3} + \rho_{iu})|\tilde{z}_{iu}|, (k_{i4} + \rho_{ir})|\tilde{z}_{ir}|]^T$.

From Lemma 1, we have $e^T (\mathcal{L} + \mathcal{L}^T) e \geq \lambda^* \|e - \frac{1_N 1_N^T}{N}(e)\|^2$. Since $\frac{1_N 1_N^T}{N}(e) = \frac{2\pi}{N} 1_N$, it follows that

$$\begin{aligned} \dot{V}_3 &\leq \sum_{i=1}^N \left\{ -\frac{\lambda_{\min}(K_{i2}) \|E_{i3}\|^2}{\sqrt{\|E_{i3}\|^2 + \Delta_{i \max}^2}} + \|h_{i3}\| \|E_{i3}\| \right\} - \frac{\lambda_{\min}(\kappa)}{2} \lambda^* \|z\|^2, \\ &\leq \sum_{i=1}^N \left\{ -\frac{\lambda_{\min}(K_{i3}) \|E_{i4}\|^2}{\sqrt{\|E_{i4}\|^2 + \Delta_{i \max}^2}} + \|h_{i3}\| \|E_{i4}\| \right\}, \end{aligned} \tag{41}$$

where $z_i = e_i - \frac{2\pi}{N} 1_N$; $z = [z_1, \dots, z_N]$; $K_{i3} = \text{diag}\{k_{i1}, U_i, k_{i2}, k_{i3}, k_{i4}, \lambda_{\min}(\kappa)\}$; $E_{i4} = [x_{ie}, y_{ie}, \psi_{ie}, \hat{z}_{iu}, \hat{z}_{ir}, z_i]^T$.

Since $\frac{\|E_{i4}\|}{\sqrt{\|E_{i4}\|^2 + \Delta_{i\max}^2}} \geq \frac{|q_{iu}|}{\theta_{i3}\lambda_{\min}(K_{i3})} + \frac{|q_{ir}|}{\theta_{i3}\lambda_{\min}(K_{i3})} + \frac{|\tilde{\beta}_{id}|}{\theta_{i3}\lambda_{\min}(K_{i3})} + \frac{(1+k_{i3}+\varrho_{iu})|\tilde{z}_{iu}|}{\theta_{i3}\lambda_{\min}(K_{i3})} + \frac{(1+k_{i4}+\varrho_{ir})|\tilde{z}_{ir}|}{\theta_{i3}\lambda_{\min}(K_{i3})} \geq \frac{\|h_{i3}\|}{\theta_{i3}\lambda_{\min}(K_{i3})}$, we have

$$\dot{V}_3 \leq \sum_{i=1}^N \left\{ -\frac{(1-\theta_{i3})\lambda_{\min}(K_{i3})\|E_{i4}\|^2}{\sqrt{\|E_{i4}\|^2 + \Delta_{i\max}^2}} \right\}, \tag{42}$$

where $0 < \theta_{i3} < 1$. Then the error subsystem (30) is ISS, and

$$\|E_{i4}(t)\| \leq \max \left\{ \varpi_{i3}(\|E_{i4}(0)\|, t), \phi_i^{q_u}(|q_{iu}|) + \phi_i^{q_r}(|q_{ir}|) + \phi_i^{\tilde{\beta}_d}(|\tilde{\beta}_{id}|) + \phi_i^{\tilde{z}_u}(|\tilde{z}_{iu}|) + \phi_i^{\tilde{z}_r}(|\tilde{z}_{ir}|) \right\}, \tag{43}$$

where ϖ_3 is a \mathcal{KL} function and $\phi_i^{q_u}(s) = \mu_i^{-1}(\sqrt{\frac{\lambda_{\max}(S_2)}{\lambda_{\min}(S_2)}} \frac{s}{\theta_{i3}\lambda_{\min}(K_{i3})})$, $\phi_i^{q_r}(s) = \mu_i^{-1}(\sqrt{\frac{\lambda_{\max}(S_2)}{\lambda_{\min}(S_2)}} \frac{s}{\theta_{i3}\lambda_{\min}(K_{i3})})$, $\phi_i^{\tilde{\beta}_d}(s) = \mu_i^{-1}(\sqrt{\frac{\lambda_{\max}(S_2)}{\lambda_{\min}(S_2)}} \frac{s}{\theta_{i3}\lambda_{\min}(K_{i3})})$, $\phi_i^{\tilde{z}_u}(s) = \mu_i^{-1}((1+k_3+\varrho_u)\sqrt{\frac{\lambda_{\max}(S_2)}{\lambda_{\min}(S_2)}} \frac{s}{\theta_{i3}\lambda_{\min}(K_{i3})})$, $\phi_i^{\tilde{z}_r}(s) = \mu_i^{-1}((1+k_4+\varrho_r)\sqrt{\frac{\lambda_{\max}(S_2)}{\lambda_{\min}(S_2)}} \frac{s}{\theta_{i3}\lambda_{\min}(K_{i3})})$ with $\mu_i(s) = \frac{s^2}{\sqrt{s^2 + \Delta_{i\max}^2}}$ and $S_{i2} = \text{diag}\{1, m_{iu}, m_{ir}\}$.

As a consequence, the following theorem presents the stability of the cascade of the subsystems (12), (25) and (30).

Theorem 1. Under Assumption 1, the cascade system formed by the subsystem (12), subsystem (25) and subsystem (30) is ISS. Besides, all error signals in the closed-loop system are uniformly ultimately bounded (UUB).

Proof. Lemmas 1–3 have shown that: subsystem (12) with state $\tilde{\beta}_{id}$ and exogenous input $\dot{\beta}_{id}$ is ISS; subsystem (25) with states $\tilde{z}_{iu}, \tilde{z}_{ir}, \tilde{W}_{iu}, \tilde{W}_{ir}$ and exogenous inputs $\varepsilon_{iu}, \varepsilon_{ir}, \tilde{W}_{iu}, \tilde{W}_{ir}$ is ISS; subsystem (30) with states $x_{ie}, y_{ie}, \psi_{ie}, \hat{z}_{iu}, \hat{z}_{ir}, e_i$, and exogenous inputs $\tilde{\beta}_{id}, \tilde{z}_{iu}, \tilde{z}_{ir}, q_{iu}, q_{ir}$ is ISS; by Lemma C.4 in [39], it follows that the complete error systems (12), (25) and (30) with states $\tilde{\beta}_{id}, \tilde{z}_{iu}, \tilde{z}_{ir}, \tilde{W}_{iu}, \tilde{W}_{ir}, x_{ie}, y_{ie}, \psi_{ie}, \hat{z}_{iu}, \hat{z}_{ir}, e_i$ and exogenous inputs $\dot{\beta}_{id}, \varepsilon_{iu}, \varepsilon_{ir}, \tilde{W}_{iu}, \tilde{W}_{ir}, q_{iu}, q_{ir}$ are ISS, i.e., there exist class \mathcal{KL} function ϖ_i and class \mathcal{K} function ϕ_i , such that

$$\|E_i(t)\| \leq \varpi_i(\|E_i(0)\|, t) + \phi_i(\|\dot{\beta}_{id}, \varepsilon_{iu}, \varepsilon_{ir}, \tilde{W}_{iu}, \tilde{W}_{ir}, q_{iu}, q_{ir}\|), \tag{44}$$

where $E_i = [\tilde{\beta}_{id}, \tilde{z}_{iu}, \tilde{z}_{ir}, \tilde{W}_{iu}, \tilde{W}_{ir}, x_{ie}, y_{ie}, \psi_{ie}, \hat{z}_{iu}, \hat{z}_{ir}, e_i]$. Note that $\dot{\beta}_{id}, \varepsilon_{iu}, \varepsilon_{ir}, \tilde{W}_{iu}, \tilde{W}_{ir}, q_{iu}$ and q_{ir} are bounded by $\beta^*, \varepsilon_{iu}^*, \varepsilon_{ir}^*, 2W_{iu}^* + \varepsilon_{i1}, 2W_{ir}^* + \varepsilon_{i2}, q_{iu}^*$ and q_{ir}^* , respectively. Then, the error signals $\tilde{\beta}_{id}, \tilde{z}_{iu}, \tilde{z}_{ir}, \tilde{W}_{iu}, \tilde{W}_{ir}, x_{ie}, y_{ie}, \psi_{ie}, \hat{z}_{iu}, \hat{z}_{ir}, e_i$ are all bounded.

4 Simulation result

Consider a networked system consisting of five USVs with the information exchange topology given in Figure 3. Suppose each vehicle is governed by a model ship CyberShip II [40], whose inertial parameters are given as $m_u = 25.8, m_v = 33.8$ and $m_r = 2.76$. The model uncertainties are given as $f_u(u, v, r) = -33.8vr - 1.0115r^2 + 0.72 + 1.33|u| + 5.87u^2 + 0.0279uv^2 + 0.0342v^2r$, $f_v(u, v, r) = 25.8u + 0.8896 + 36.5|v| + 0.805|r|$ and $f_r(u, v, r) = -33.8uv - 1.115ur - 25.8uv + 1.90 - 0.08|v| + 0.75|r| + 0.0156ur^2 + 0.0278urv^3$. Without loss of generality, environmental disturbances are introduced into the model: $\tau_{uw} = -0.2 \cos(1.0t) \cos(1.5t)$, $\tau_{vw} = 0.01 \sin(0.1t)$ and $\tau_{rw} = -0.3 \sin(2.0t) \cos(2.3t)$. A reference closed curve is given by $x_d(\theta) = 50 \cos \theta, y_d(\theta) = 60 \sin \theta$. Select the control parameters as follows: $\Delta_i = 5, k_{i1} = 0.2, \Delta_{ix} = 2, k_{i2} = 0.2, \Delta_{iy} = 2, k_{i3} = 1, \Delta_{iu} = 0.8, k_{i4} = 0.7, \Delta_{ir} = 0.8, \rho_{iu} = 25, \rho_{ir} = 25, \gamma_{iu} = 1, \gamma_{ir} = 1, \Gamma_{iu} = 100, \Gamma_{ir} = 100, \kappa_i = 0.005$.

Simulation results are shown in Figures 4–7. Figure 4 shows that a symmetric formation formed by the five vehicles along a closed curve can be reached. As z_i is bounded, e_i will nearly converge to $2\pi/N$ with $N = 5$ herein and from (29), the parameter updating velocity $\dot{\theta}_i$ in steady state will be $\kappa_i(2\pi/N)$. As a result, the surge speed for each USV in steady state is $\kappa_i u_{id}^*(2\pi/N)$. The along-track error x_{ie} and

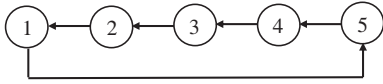


Figure 3 Communication topology.

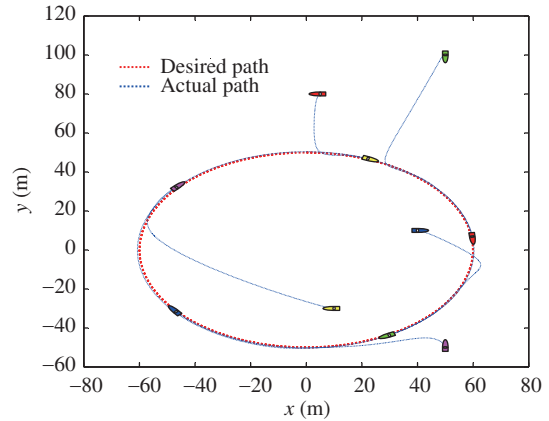


Figure 4 (Color online) Path following performance.

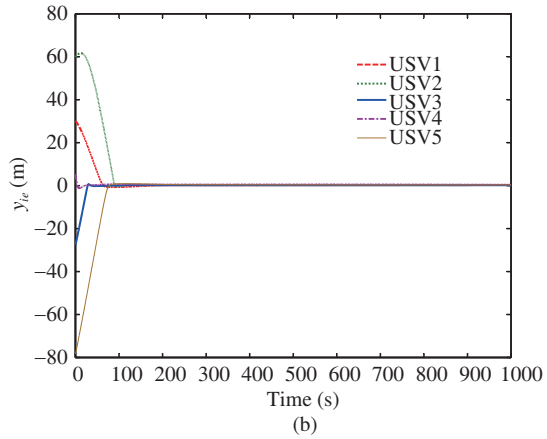
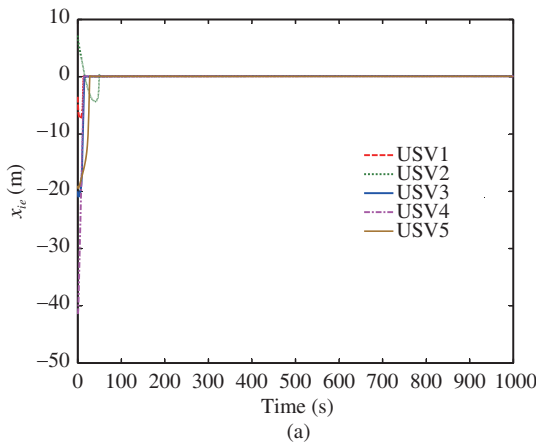


Figure 5 (Color online) Tracking errors. (a) Along-track errors; (b) cross-track errors.

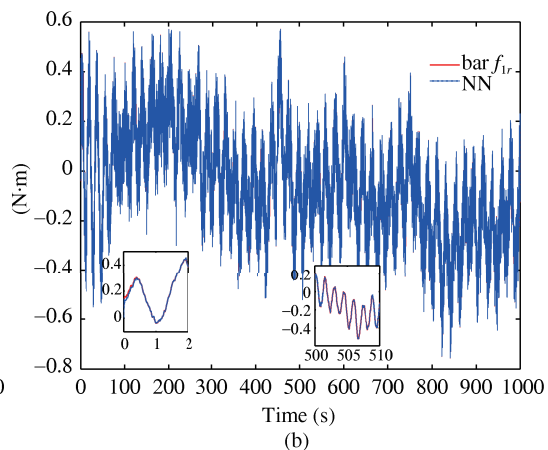
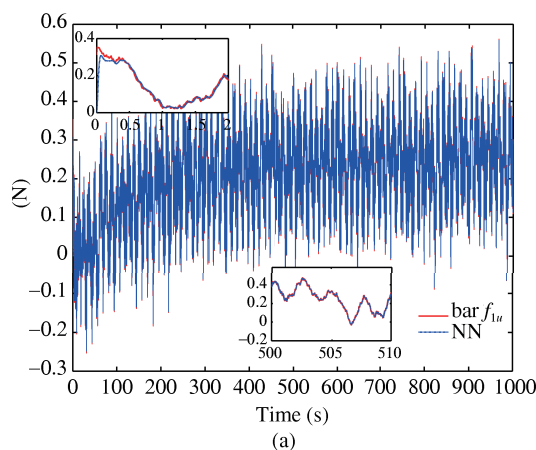


Figure 6 (Color online) The estimation performance of neural networks. (a) The estimation of \bar{f}_{1u} ($\text{bar}f_{1u} = \bar{f}_{1u}$); (b) the estimation of f_{1r} ($\text{bar}f_{1r} = f_{1r}$).

cross-track error y_{ie} are plotted in Figure 5. It can be seen that the tracking errors are bounded to a small neighborhood of the origin. The estimation performance of neural networks is shown in Figure 6, where it demonstrates that the uncertainties are efficiently compensated by the proposed neural networks.

To better show the efficiency of the proposed saturated coordinated controller (9), (14), (16), (22), (24), (29), comparison study with the predictor-based neural control method [41] is made. The coordinated

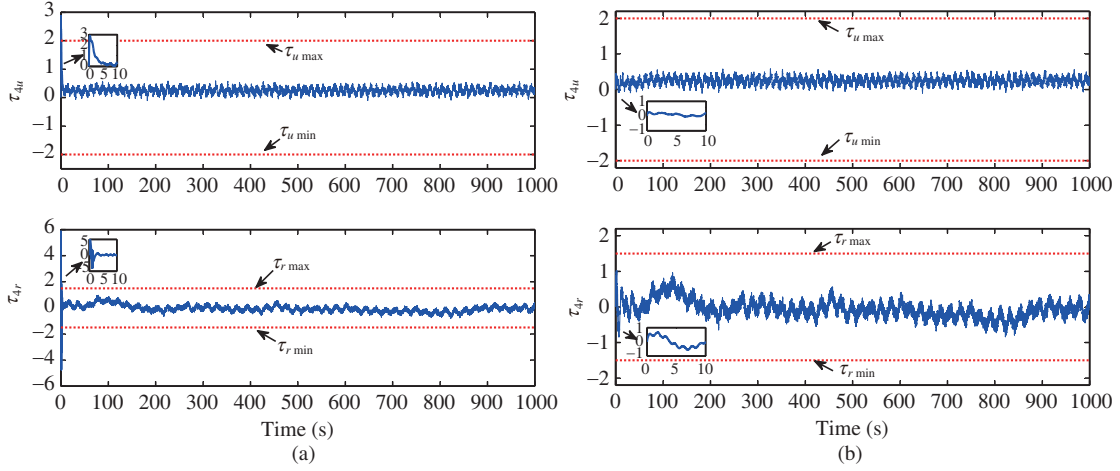


Figure 7 (Color online) Comparisons of control inputs using different methods. (a) Control inputs of the control method in [41]; (b) control inputs of the proposed method.

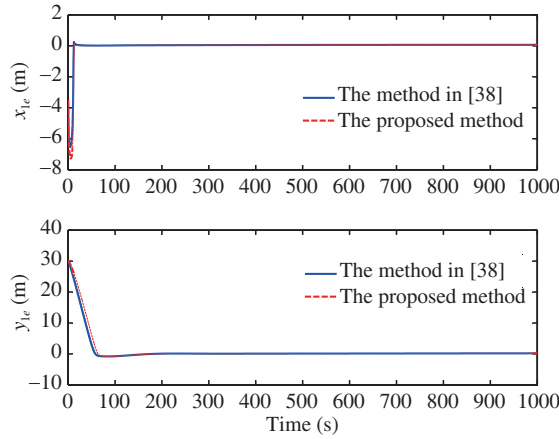


Figure 8 (Color online) Comparisons of tracking errors.

controller using the predictor-based neural control method is given by (16), (24), (29) and

$$\begin{cases} \alpha_{\psi_i} = \psi_{id} + \arctan\left(-\frac{y_{ie}}{\Delta_i}\right), \\ \alpha_{U_i} = -k_{i1}x_{ie} + u_{id}^*\dot{\theta}_i + 2U_i\sin^2\left(\frac{\psi_{iW} - \psi_{id}}{2}\right) - \hat{z}_{iu}, \\ \alpha_{r_i} = -k_{i2}\psi_{ie} - \hat{\beta}_{id} + \dot{\alpha}_{\psi_i} - \frac{y_{ie}Q_i}{\psi_{ie}} - \hat{z}_{ir}, \\ \tau_{iu} = -k_{i3}\hat{z}_{iu} - \hat{W}_{iu}^T\sigma_{iu}(\xi_{iu}), \\ \tau_{ir} = -k_{i4}\hat{z}_{ir} - \hat{W}_{ir}^T\sigma_{ir}(\xi_{ir}). \end{cases} \quad (45)$$

Figure 7 depicts the comparison of control inputs using the predictor-based neural control method in [41] and the proposed method. Figure 7(a) shows that the control inputs of the predictor-based neural control may exceed the desired bound in transient process. This may be not implementable by actuators with limited energy. By contrast, Figure 7(b) verifies that control inputs of the proposed controller are bounded within 2 N and 1.5 N · m. The comparison of tracking errors using the predictor-based neural control method in [41] and the proposed method is shown in Figure 8. It can be observed that in the steady state, the tracking errors of both methods are almost the same; in the transient state, the tracking errors of the method in [41] are a little smaller than those of the proposed method. However, compared with the method given in [41], the proposed method is able to obtain acceptable performance without violating the input constraints.

5 Conclusion

This paper addressed the coordinated control problem of multiple underactuated USVs over a closed curve while holding a symmetric formation. The kinematic control law is designed based on a reduced-order extended state observer, which is utilized to compensate for the effort of the sideslip. The bounded kinetic control law is developed by combining the saturated function, the projection operator, and the dynamic surface control design method. The parameter cyclic pursuit approach is proposed to guarantee that the vehicles are evenly spaced over the closed curve. The input-to-state stability of the closed-loop system is analyzed via cascade theory. Comparison studies are given to illustrate the efficacy of the proposed method. We discuss some possible further works. First, time delays are pervasive in engineering systems, and it is desirable to investigate the coordinated control problem of USVs in the presence of time delays. Second, it will be interesting to implement the proposed coordinated algorithm in a real world multi-vehicle system.

Acknowledgements This work was supported in part by National Natural Science Foundation of China (Grant Nos. 61673081, 51579023), China Postdoctoral Science Foundation (Grant No. 2015M570247), Fundamental Research Funds for the Central Universities (Grant No. 3132016313), National Key Research and Development Program of China (Grant No. 2016YFC0301500), and High Level Talent Innovation and Entrepreneurship Program of Dalian (Grant No. 2016RQ036).

Conflict of interest The authors declare that they have no conflict of interest.

References

- 1 Liu Z, Zhang Y, Yu X, et al. Unmanned surface vehicles: an overview of developments and challenges. *Ann Rev Contr*, 2016, 41: 71–93
- 2 Fahimi F. Sliding-mode formation control for underactuated surface vessels. *IEEE Trans Robot*, 2007, 23: 617–622
- 3 Kyrkjebø E, Pettersen K Y, Wønsted M, et al. Output synchronization control of ship replenishment operations: theory and experiments. *Contr Eng Pract*, 2007, 15: 741–755
- 4 Schoerling D, Kleeck C V, Fahimi F, et al. Experimental test of a robust formation controller for marine unmanned surface vessels. *Auton Robots*, 2009, 28: 213–230
- 5 Mahacek P, Mas I, Petrovic O, et al. Cluster space control of autonomous surface vessels. *Mar Tech Soc J*, 2009, 43: 13–20
- 6 Arrichiello F, Das J, Heidarsson H, et al. Multi-robot collaboration with range-limited communication: experiments with two underactuated ASVs. In: *Field and Service Robotics*. Berlin: Springer, 2010. 443–453
- 7 Peng Z, Hu X, Wang D. Robust adaptive formation control of underactuated autonomous surface vehicles with uncertain dynamics. *IET Contr Theory Appl*, 2011, 5: 1378–1387
- 8 Peng Z, Wang D, Chen Z, et al. Adaptive dynamic surface control for formations of autonomous surface vehicles with uncertain dynamics. *IEEE Trans Contr Syst Tech*, 2013, 21: 513–520
- 9 Ihle I-A F, Jouffroy J, Fossen T I. Formation control of marine surface craft: a lagrangian approach. *IEEE J Ocean Eng*, 2006, 31: 922–934
- 10 Ihle I A F, Jouffroy J, Fossen T I. Formation control of marine surface craft: a lagrangian approach. *IEEE J Ocean Eng*, 2006, 31: 922–934
- 11 Dong W. Cooperative control of underactuated surface vessels. *IET Contr Theory Appl*, 2010, 4: 1569–1580
- 12 Mahacek P, Kitts C A, Mas I. Dynamic guarding of marine assets through cluster control of automated surface vessel fleets. *IEEE/ASME Trans Mech*, 2012, 17: 65–75
- 13 Elkins L, Sellers D, Monach W R. The autonomous maritime navigation (AMN) project: field tests, autonomous and cooperative behaviors, data fusion, sensors, and vehicles. *J Field Robot*, 2010, 27: 790–818
- 14 Peng Z, Wang D, Shi Y, et al. Containment control of networked autonomous underwater vehicles with model uncertainty and ocean disturbances guided by multiple leaders. *Inf Sci*, 2015, 316: 163–179
- 15 Peng Z H, Wang D, Li T S. Predictor-based neural dynamic surface control for distributed formation tracking of multiple marine surface vehicles with improved transient performance. *Sci China Inf Sci*, 2016, 59: 092210
- 16 Ihle I-A F, Arcaç M, Fossen T I. Passivity-based designs for synchronized path-following. *Automatica*, 2007, 43: 1508–1518
- 17 Almeida J, Silvestre C, Pascoal A. Cooperative control of multiple surface vessels in the presence of ocean currents and parametric model uncertainty. *Int J Robust Nonlin Contr*, 2010, 20: 1549–1565
- 18 Almeida J, Silvestre C, Pascoal A M. Cooperative control of multiple surface vessels with discrete-time periodic communications. *Int J Robust Nonlin Contr*, 2011, 22: 398–419
- 19 Wang H, Wang D, Peng Z, et al. Adaptive dynamic surface control for cooperative path following of underactuated

- marine surface vehicles via fast learning. *IET Contr Theory Appl*, 2013, 7: 1888–1898
- 20 Wang H, Wang D, Peng Z. Neural network based adaptive dynamic surface control for cooperative path following of marine surface vehicles via state and output feedback. *Neurocomputing*, 2014, 133: 170–178
 - 21 Wang H, Wang D, Peng Z H. Adaptive dynamic surface control for cooperative path following of marine surface vehicles with input saturation. *Nonlin Dynam*, 2014, 77: 107–117
 - 22 Peng Z H, Wang J, Wang D. Containment maneuvering of marine surface vehicles with multiple parameterized paths via spatial-temporal decoupling. *IEEE/ASME Trans Mech*, 2017, 22: 1026–1036
 - 23 Peng Z H, Wang J, Wang D. Distributed containment maneuvering of multiple marine vessels via neurodynamics-based output feedback. *IEEE Trans Ind Electron*, 2017, 64: 3831–3839
 - 24 Liu L, Wang D, Peng Z H. Coordinated path following of multiple underactuated marine surface vehicles along one curve. *ISA Trans*, 2016, 64: 258–268
 - 25 Liu L, Wang D, Peng Z H, et al. Modular adaptive control for LOS-based cooperative path maneuvering of multiple underactuated autonomous surface vehicles. *IEEE Trans Syst Man Cyber Syst*, 2017, in press. Doi: 10.1109/TSMC.2017.2650219
 - 26 Peng Z H, Wang J, Wang D. Distributed maneuvering of autonomous surface vehicles based on neurodynamic optimization and fuzzy approximation. *IEEE Trans Contr Syst Tech*, 2017, in press. Doi: 10.1109/TCST.2017.2699167
 - 27 Peng Z H, Wang J. Output-feedback path-following control of autonomous underwater vehicles based on an extended state observer and projection neural networks. *IEEE Trans Syst Man Cyber Syst*, 2017, in press. Doi: 10.1109/TSMC.2017.2697447
 - 28 Zhang F, Leonard N E. Coordinated patterns of unit speed particles on a closed curve. *Syst Contr Lett*, 2007, 56: 397–407
 - 29 Paley D, Zhang F, Leonard N. Cooperative control for ocean sampling: the glider coordinated control system. *IEEE Trans Contr Syst Tech*, 2008, 16: 735–744
 - 30 Chen Y-Y, Tian Y-P. A curve extension design for coordinated path following control of unicycles along given convex loops. *Int J Contr*, 2011, 84: 1729–1745
 - 31 Chen Y-Y, Tian Y-P. Coordinated adaptive control for three-dimensional formation tracking with a time-varying orbital velocity. *IET Contr Theory Appl*, 2013, 7: 646–662
 - 32 Chen Y-Y, Wei P. Coordinated adaptive control for coordinated path-following surface vessels with a time-invariant orbital velocity. *IEEE/CAA J Autom Sin*, 2014, 1: 337–346
 - 33 Chen Y-Y, Tian Y-P. Coordinated path following control of multi-unicycle formation motion around closed curves in a time-invariant flow. *Nonlin Dynam*, 2015, 81: 1005–1016
 - 34 Chen Y-Y, Tian Y-P. Formation tracking and attitude synchronization control of underactuated ships along closed orbits. *Int J Robust Nonlin Contr*, 2015, 25: 3023–3044
 - 35 Ceragioli F, Persis C D, Frasca P. Discontinuities and hysteresis in quantized average consensus. *Automatica*, 2011, 47: 1916–1928
 - 36 Fossen T I. *Handbook of Marine Craft Hydrodynamics and Motion Control*. Hoboken: John Wiley & Sons Ltd, 2011
 - 37 Pomet J B, Praly L. Adaptive nonlinear regulation: estimation from the lyapunov equation. *IEEE Trans Autom Contr*, 1992, 37: 729–740
 - 38 Lavretsky E, Gadiant R, Gregory I M. Predictor-based model reference adaptive control. *J Guid Contr Dynam*, 2010, 33: 1195–1201
 - 39 Krstić M, Kanellakopoulos I, Kokotovic P. *Nonlinear and Adaptive Control Design*. Hoboken: John Wiley & Sons, 1995
 - 40 Skjetne R, Fossen T I, Kokotović P V. Adaptive maneuvering, with experiments, for a model ship in a marine control laboratory. *Automatica*, 2005, 41: 289–298
 - 41 Peng Z H, Wang D, Wang J. Predictor-based neural dynamic surface control for uncertain nonlinear systems in strict-feedback form. *IEEE Trans Neural Netw Learn Syst*, 2016, in press. doi: 10.1109/TNNLS.2016.2577342